

JAN 26 1977

NOT TO BE REMOVED FROM LIBRARY

TECHNICAL MEMORANDUMS  
NATIONAL ADVISORY COMMITTEE FOR AERONAUTICS

---

NO. 1060

---

PROFILE MEASUREMENTS DURING CAVITATION

By O. Walchner

Reprint of a report read before the Congress on  
Hydromechanical Problems of Ship Propulsion at  
Hamburg, May 18 and 19, 1932

---

*Straight Document file*

---

Washington  
January 1944

NACA LIBRARY  
LANGLEY MEMORIAL AERONAUTICAL  
LABORATORY  
Langley Field, Va.



## NATIONAL ADVISORY COMMITTEE FOR AERONAUTICS

## TECHNICAL MEMORANDUM NO. 1060

## PROFILE MEASUREMENTS DURING CAVITATION\*

By O. Walchner

One of the problems of modern cavitation research is the experimental determination of the wing loads on airfoils during cavitation. Such experiments were made on various airfoils with the support of the naval ministry at the Kaiser Wilhelm Institute for Flow Research at Göttingen.

The experimental setup is a vertical closed circular channel as shown in figure 1.\*\* The testing medium is water. An 18-horsepower centrifugal pump provides for the circulation of the water and is placed in the deepest point in order to protect it against cavitation. After passing through a unidirector the water passes through a cone into the test section and is pumped through a diffuser into the surge tank. The purpose of the deflector vanes is to guide the flow, coming from the pump upward, along the tank wall, so that any entrained gas bubbles are eliminated. By evacuating the air space above the water level in the tank the pressure in the test section can be lowered at will and hence any cavitation number — that is, any condition of cavitation — even those at low speeds can be obtained. The cavitation number is defined as  $(p - p_D)/q$

where

$p$  pressure of undisturbed flow

$p_D$  vapor tension of water at the temperature under consideration.

$q = \frac{\rho}{2} v^2$  dynamic pressure of undisturbed flow

$\rho$  density

$v$  velocity of undisturbed flow

The speed can be varied by means of the slide valve

\*"Profilmessung bei Kavitation." From reprint of paper presented at the Conference on hydromechanische Probleme des Schiffsantriebs, Hamburg, May 18 and 19, 1932.

\*\*The plan of the testing section and balance which are sketched only schematically are by Dr.-Ing. H. Mueller.

in back of the pump. Pressure and dynamic pressure in the undisturbed flow are recorded in the test section ahead of the airfoil, and the values are calculated for the free flow section adjacent to the wing profile and cavitation layer by means of Bernoulli's law and the continuity equation. It was found that this method affords the best means of determining the principal effect of the tunnel walls. The contraction of the thin tunnel section  $\Delta f$  caused by the wing profile and cavitation layer depends upon the airfoil section, angle of attack, and cavitation number, and is to be determined for each case. Another effect of the horizontal tunnel walls is the creation of a streamline curvature at the profile. This effect can be calculated by means of an approximation theory of Professor Prandtl. (See reference 1.) The lift coefficient  $c_a$  measured in the rectangular tunnel at angle of attack  $\alpha$  corresponds to the angle of attack  $\alpha + \Delta\alpha$  in infinite flow, where

$$\Delta\alpha = \frac{\pi}{96} \left( \frac{t}{H} \right)^2 c_a$$

( $t$  wing chord,  $H$  tunnel height). The effect of the vertical sides, which may produce a kind of induced drag, was not investigated. The wing loads are measured on a spring balance. The model airfoil is mounted on a disk which is flush with the tunnel wall and is connected with the arm of the balance. With this setup the drag of the disk as well as of the airfoil is measured, and therefore the disk must subsequently be measured by itself and its effect taken into account. A labyrinth behind the disk is intended to prevent flows in the housing of the balance which works under water. The model airfoil extends almost from wall to wall. A gap of about 1/10 millimeter is necessary for balance clearance. The disturbance of the two-dimensional flow created by this small gap was disregarded. A window afforded the means of observing the cavitation. The experiments were made at Reynolds

numbers ranging from  $\frac{v t}{\nu} = 3 \times 10^5$  to  $5 \times 10^5$ .

( $t$  wing chord,  $v$  speed,  $\nu$  kinematic viscosity).

Figure 2 illustrates the three different types of cavitation phenomena observed.

Case 1.— Suction side cavitation starts at leading

edge, when the forward stagnation point lies on the pressure side and the lowest pressures, on the suction side, caused by flow from the pressure side around the leading edge occur directly at the leading edge.

Case 2.— Suction side cavitation starts at profile center when the forward stagnation point lies on the leading edge itself, so that the water flows smoothly\* over it. Likewise, suction side cavitation of case 2 only can form if the forward stagnation point lies on the suction side.

Case 3.— Pressure-side cavitation starting from the leading edge occurs only when the forward stagnation point lies on the suction side and the flow around the leading edge comes from the suction side.

For flow without cavitation the position of the forward stagnation point depends upon the airfoil section and the angle of attack. In potential flow the flow around circular segment sections is smooth\* at  $\alpha_{\infty} = 0^{\circ}$ ; in a real fluid this condition obtains at a slightly greater angle as a result of circulation decrease due to the dead water. At greater angles of attack, beyond the angle of smooth flow, the forward stagnation point lies on the pressure side; at smaller angle of attack on the suction side. Once cavitation has begun, the stagnation points begin to shift conformably to the change in circulation caused by the cavitation even at constant angle of attack. This explains why at the same angle of attack case 1 changes to case 2 for decreasing cavitation numbers: that is, when the growing suction-side cavitation reduces the circulation to the extent that the forward stagnation point shifts on the leading edge. Indeed, it is even possible that, as a result of continuously increasing suction-side cavitation, the circulation is decreased further and the forward stagnation points shifts to the suction side, so that case 3 as well as case 2 may occur at positive  $\alpha$ .

The results and observations on three circular segments of various thickness are shown in figures 3, 4, and 5; on the left are the forces on the wing, on the right are the profiles investigated, together with their cavitation diagrams. The data for lift and drag are given in tables I to III.

---

\*smooth; forward pressure point directly on leading edge.

In the cavitation diagrams the length of the cavitation layer has been plotted for two-dimensional flow and infinite extent of fluid against angle of attack  $\alpha_\infty$  and against the cavitation number. The solid curves indicate suction-side cavitation starting from the leading edge (i.e., case 1). Parameter  $X$  indicates the length of the cavitation measured in percent of chord from the leading edge. The dotted curves denote suction-side cavitation starting at profile center and extending  $X$  percent of the chord. The dash-dot curves mark the beginning of the suction-side cavitation (i.e., case 2). The dashed curves give the pressure side cavitation starting at the leading edge and extending to  $X$  percent of the chord (i.e., case 3). The cavitation diagrams show how, at constant  $\alpha$ , the various cavitation conditions follow one another for changing cavitation number. To illustrate: at  $\alpha_\infty = 1^\circ$  on the thinnest profile the cavitation starts at cavitation number 0.3 as case 1 and temporarily spreads as such as the cavitation factor drops. At 0.18 case 1 changes to case 2, the cavitation stops at the leading edge and starts near the profile center, the forward stagnation point has now reached the leading edge, so that the flow is smooth. At a cavitation number of 0.11 cavitation starts again at the leading edge and, to be sure, on the pressure side, a visible sign that the forward stagnation point has gone over to the suction side. Case 3 is added to case 2. The range of positive  $d$  within which pressure-side cavitation is thus produced, grows with the thickness of the profile. Thus the diagram of the thickest profile in figure 5 shows this range particularly extended.

From the available corrosion tests it is concluded that corrosion by cavitation occurs at the position of the compression shock. Accordingly, there is danger of corrosion in the diagonally shaded zones of the cavitation diagrams where the compression shock lies on the profile. Another zone where cavitation is disagreeably noticeable is indicated by the horizontal hatching. Here the form of the cavitation layer is particularly unstable. This is associated with periodic changes in the wing loads, which may produce wing flutter.

Next, consider forces on the wing. These are presented in the customary polar form, and the well-known definitions hold:

$$C_a = \frac{A}{q F}, \quad C_w = \frac{W}{q F}$$

where

A lift

W drag

q dynamic pressure

F wing area

The solid curves represent the polars without cavitation. The thin curves are the polars with constant cavitation number. Each planing angle is designated by a symbol. A comparison of the different polars of an airfoil discloses the drop in lift to be particularly responsible for the deterioration of the airfoil characteristics by cavitation. The dashed curves give the forces at constant angle of attack and at various cavitation numbers. Following these dashed curves it was found that in each case where cavitation begins, as case 1, an improved  $W/A$  ratio occurs as a result of an increase in lift and a decrease in drag. Considering the cavitation layer as a deformation of the profile the lift increases must be explained by the greater profile number. Concerning the two drag components, the frictional drag decreases, the profile drag increases as a result of expanding dead water. The preponderance of either component depends upon the thickness of the cavitation layer. Thus, thin layers manifest a perceptible drag decrease; while, for thicker layers - that is, at greater angles of attack - the increase in profile drag predominates. The  $W/A$  ratio in cavitation of case 1 deteriorates only when the cavitation has extended to beyond the profile center. Depending therefore upon the angle of attack, there exists, for case 1, a greater or lesser interval in cavitation number between start of cavitation and deterioration of the  $W/A$  ratio.

If cavitation starts as case 2, the  $W/A$  ratio, as well as the beginning of cavitation, drop. This is seen plainly in the case of the two thicker airfoils of figures 4 and 5.

With cavitation starting as case 3 the conditions are similar to that of case 1.

Professor Betz (reference 2) has established an approximate theory for the behavior of lift and drag under conditions of fully developed suction-side cavitation of case 1. According to the theory the lift coefficient is

$$c_a = \frac{\pi}{2} \alpha + \frac{p - p_D}{q}$$

The first part on the right-hand side represents Kirchhoff's lift coefficient for a flat plate at small  $\alpha$  in turbulent flow with free jet limits, where the pressure in the dead water space is the same as in the undisturbed fluid. The second part, the cavitation number, gives the additional lift, which is due to the fact that during cavitation a lesser pressure — that is, the vapor pressure — and not the pressure of undisturbed flow, prevails in the dead water section on the suction side. Since the resultant pressure force is at right angles to the flat pressure side the drag consists of the tangential component of the lift and the frictional drag on the pressure side; hence;

$$c_w = c_a \times \alpha + 0.004$$

According to Betz, these figures are applicable not only to flat plates but to any airfoils with flat pressure sides, provided the cavitation starts at the leading edge and extends to the trailing edge — that is, envelopes the entire suction side of a cavitation layer; thus shape becomes unimportant. As long as this assumption of the theory is complied with — that is, as long as case 1 of cavitation exists — the experiments confirm the theory. The lift coefficients are in complete accord with theory; the measured drag coefficients are slightly higher at low cavitation numbers than the theory stipulates. In all other cavitation cases, where the theoretical premise breaks down, the profile characteristics become worse, as was pointed out by Professor Betz. The drag increases; the lift drops rapidly with diminishing cavitation number, especially for pressure-side cavitation at positive angles of attack.

The points in figures 3 to 5 indicate averages of individual tests series and are not test points. Figure 6 presents the individual test points of a test series with the thinnest airfoil at constant  $\alpha_\infty = 3^\circ$ . Lift and drag

coefficients are plotted against cavitation number. The dashed lines represent the approximate theory of Betz, whose assumptions are borne out by the test series.

Figure 7 illustrates parts of the three cavitation plots of the three airfoil models investigated. The profiles are indicated by their thickness ratio  $F/t$  ( $F$  maximum thickness at profile center,  $t$  wing chord).

The shaded zones of the angles of attack and cavitation figures indicate the danger zones of corrosion or severe compression shocks. The solid lines indicate the position of the best  $W/A$ ; it is seen that, at low cavitation numbers, of special significance for high-speed propellers, the best  $W/A$  ratios lie precisely outside the danger zones.

The solid curves in figure 8 give the cavitation beginnings of the three profiles as functions of cavitation number and lift. Each curve consists of three branches; in the lower branch, cavitation starts as case 3; in the middle, as case 2; and in the upper, as case 1. As anticipated, the profiles are least responsive to cavitation in the zone of smooth flow; while at either side of the smooth flow condition cavitation starts at much higher cavitation numbers. The dashed curve gives a relation (calculated for potential flow) between the beginning of cavitation and lift coefficient  $c_{a_0}$  for smooth flow ( $\alpha_\infty = 0^\circ$ ). A cyclic flow with circulation was conformably transformed by means of the K arman-Trefftz function (reference 3) to flow about profiles of various thicknesses, and the cavitation number was computed as dependent upon the lift at which cavitation starts. This gives as a second approximation

$$\frac{P - P_D}{q} = 1041 c_{a_0} + 0.213 c_{a_0}^2$$

The terms of the third order may be disregarded, if normal profile thicknesses are assumed.

The dashed curve passes very closely to the measured values for  $\alpha_\infty = 0^\circ$ . It affords, at least for thin profiles, in actual flow, a practical relation for rough calculations between a given cavitation number and the highest possible lift coefficient attainable without cavitation at smooth flow. As the profile thickness increases

(i.e., by increasing angle at the leading edge) the zone in which cavitation of type 2 begins, becomes greater. The highest lift coefficients still obtainable without cavitation become even greater than our formula indicates.

Translation by J. Vanier,  
National Advisory Committee  
for Aeronautics.

#### REFERENCES

1. Schiller, Ludwig: Handbuch der Experimentalphysik. Bd. 4, 2. Teil, 1932, chap. VI, sec. 2.
2. Betz, A. Einfluss der Kavitation auf die Leistung von Schiffsschrauben. Verhandlungen des III. Internationalen Kongresses für technische Mechanik Stockholm, 1930, Bd. I, p. 411.
3. von Kàrmàn, Th., and Trefftz, E.: Potentialströmung um gegebene Tragflächenquerschnitte. Z.F.M., IX. Jahrg., Heft 17 u. 18, Sept. 28, 1918, pp. 111-116.

TABLE I.- LIFT-DRAG COEFFICIENTS,  $f:t = 0.0385$ .

$\alpha_{\infty} \backslash \frac{p-p_D}{q}$		0,0	0,1	0,2	0,3	0,4	0,5	0,6	0,7	0,8	0,9	1,0	1,1	1,2	1,3	1,4
6°	$C_L$	0,15	0,26	0,37	0,47	0,56	0,64	0,71	0,76	0,79	0,79	0,76	0,76	0,75	0,74	0,73
	$C_W$	0,023	0,034	0,044	0,052	0,059	0,064	0,069	0,070	0,068	0,053	0,049	0,048	0,047	0,047	0,047
5°	$C_L$	0,13	0,23	0,34	0,44	0,53	0,60	0,66	0,70	0,70	0,67	0,67	0,66	0,66		
	$C_W$	0,020	0,029	0,036	0,042	0,046	0,051	0,054	0,044	0,035	0,033	0,034	0,035	0,035		
4°	$C_L$	0,11	0,20	0,30	0,41	0,50	0,56	0,61	0,60	0,57	0,57					
	$C_W$	0,016	0,023	0,027	0,032	0,036	0,038	0,032	0,021	0,023	0,024	0,024				
3°	$C_L$	0,08	0,17	0,28	0,38	0,46	0,50	0,50	0,47	0,46						
	$C_W$	0,012	0,017	0,020	0,024	0,027	0,018	0,014	0,015	0,016	0,016					
2°	$C_L$	0,05	0,17	0,28	0,37	0,41	0,37	0,37								
	$C_W$	0,013	0,014	0,016	0,016	0,011	0,012	0,012								
1°	$C_L$	0,00	0,15	0,27	0,28	0,28										
	$C_W$	0,012	0,012	0,011	0,010	0,010										
0°	$C_L$	0,00	0,09	0,17	0,17											
	$C_W$	0,010	0,010	0,009	0,009											
-1°	$C_L$	0,00	-0,01	0,07	0,07	0,08	0,08									
	$C_W$	0,009	0,008	0,009	0,010	0,010										
-2°	$C_L$	-0,01	-0,04	-0,14	-0,05	-0,03	-0,03	-0,02	-0,02							
	$C_W$	0,011	0,011	0,012	0,012	0,012	0,012	0,012	0,012							
-3°	$C_L$	-0,02	-0,07	-0,16	-0,26	-0,18	-0,15	-0,14	-0,13	-0,13						
	$C_W$	0,013	0,015	0,015	0,016	0,016	0,017	0,017	0,017	0,017						

TABLE II.- LIFT-DRAG COEFFICIENTS,  $f:t = 0.0735$ .

$\alpha_{\infty} \backslash \frac{p-p_D}{q}$		0,0	0,1	0,2	0,3	0,4	0,5	0,6	0,7	0,8	0,9	1,0	1,1	1,2	1,3	1,4
6°	$C_L$	0,17	0,25	0,35	0,46											
	$C_W$	0,031	0,037	0,046	0,054											
5°	$C_L$	0,13	0,24	0,33	0,44	0,54	0,61	0,63	0,75	0,81	0,83	0,76	0,74	0,74	0,74	0,74
	$C_W$	0,028	0,038	0,040	0,046	0,049	0,050	0,049	0,046	0,034	0,023	0,025	0,027	0,029	0,029	0,029
4°	$C_L$	0,08	0,19	0,30	0,41	0,52	0,61	0,68	0,73	0,72	0,67	0,66	0,66	0,66		
	$C_W$	0,025	0,029	0,034	0,038	0,039	0,036	0,030	0,021	0,018	0,021	0,023	0,023	0,023		
3°	$C_L$	0,04	0,14	0,27	0,38	0,50	0,59	0,60	0,57	0,57	0,57					
	$C_W$	0,023	0,026	0,030	0,032	0,030	0,023	0,017	0,018	0,018	0,018					
2°	$C_L$	0,01	0,08	0,22	0,36	0,47	0,50	0,50	0,50							
	$C_W$	0,020	0,023	0,027	0,028	0,023	0,013	0,013	0,013							
1°	$C_L$	-0,03	0,02	0,18	0,32	0,41	0,43	0,43								
	$C_W$	0,018	0,021	0,024	0,024	0,017	0,012	0,012								
0°	$C_L$	-0,03	-0,03	0,14	0,29	0,35	0,35	0,35								
	$C_W$	0,023	0,023	0,022	0,019	0,012	0,011	0,011								
-1°	$C_L$	-0,03	-0,04	0,08	0,24	0,28	0,28									
	$C_W$	0,027	0,024	0,020	0,015	0,011	0,012									
-2°	$C_L$	-0,03	-0,05	0,00	0,16	0,19	0,19									
	$C_W$	0,032	0,028	0,021	0,014	0,013	0,014									
-3°	$C_L$	-0,05	-0,06	-0,07	-0,02	0,06	0,08	0,09	0,10	0,10	0,10					
	$C_W$	0,036	0,033	0,028	0,020	0,016	0,017	0,017	0,017	0,018	0,018	0,018				

TABLE III.- LIFT-DRAG COEFFICIENTS,  $f:t = 0.1475$ .

$\alpha_{\infty} \backslash \frac{p-p_D}{q}$		0,0	0,1	0,2	0,3	0,4	0,5	0,6	0,7	0,8	0,9	1,0
5°	$C_L$	0,07	0,18	0,29	0,40	0,52	0,62	0,72	0,81	0,88	0,89	0,89
	$C_W$	0,046	0,059	0,067	0,072	0,075	0,074	0,070	0,060	0,043	0,040	0,040
4°	$C_L$	-0,02	0,10	0,22	0,35	0,47	0,58	0,70	0,79	0,84	0,85	0,85
	$C_W$	0,038	0,051	0,061	0,067	0,069	0,068	0,062	0,053	0,057	0,054	0,054
3°	$C_L$	-0,04	0,09	0,17	0,30	0,43	0,55	0,66	0,74	0,81	0,81	
	$C_W$	0,042	0,049	0,058	0,063	0,063	0,061	0,053	0,043	0,032	0,030	
2°	$C_L$	-0,04	-0,04	0,11	0,26	0,38	0,51	0,62	0,70	0,74	0,75	
	$C_W$	0,047	0,050	0,056	0,059	0,058	0,053	0,045	0,033	0,027	0,026	
1°	$C_L$	-0,04	-0,05	0,03	0,19	0,34	0,46	0,57	0,65	0,68	0,68	
	$C_W$	0,051	0,054	0,054	0,056	0,055	0,049	0,040	0,026	0,022	0,022	
0°	$C_L$	-0,05	-0,06	-0,02	0,14	0,29	0,42	0,52	0,60	0,61	0,61	
	$C_W$	0,057	0,059	0,054	0,055	0,053	0,047	0,036	0,024	0,020	0,020	
-1°	$C_L$	-0,06	-0,06	-0,06	0,09	0,24	0,37	0,47	0,53	0,54	0,54	
	$C_W$	0,061	0,065	0,061	0,055	0,051	0,045	0,034	0,023	0,022	0,022	
-2°	$C_L$	-0,06	-0,06	-0,07	0,03	0,18	0,30	0,40	0,46	0,47	0,47	
	$C_W$	0,066	0,071	0,067	0,057	0,051	0,048	0,033	0,025	0,025	0,025	
-3°	$C_L$	-0,06	-0,07	-0,07	-0,03	0,11	0,23	0,32	0,38	0,38	0,38	
	$C_W$	0,070	0,074	0,074	0,065	0,054	0,043	0,035	0,025	0,022	0,022	
-4°	$C_L$	-0,06	-0,07	-0,07	-0,07	0,03	0,16	0,25	0,28	0,28	0,28	
	$C_W$	0,074	0,081	0,081	0,074	0,060	0,047	0,036	0,028	0,028	0,028	

- k Centrifugal pump
- g Honeycomb
- dü Cone
- m Test section
- di Diffusor
- u Guide vanes
- si Slide valve
- mf Model airfoil
- se Disk
- w Balance
- l Labryinth
- s Window

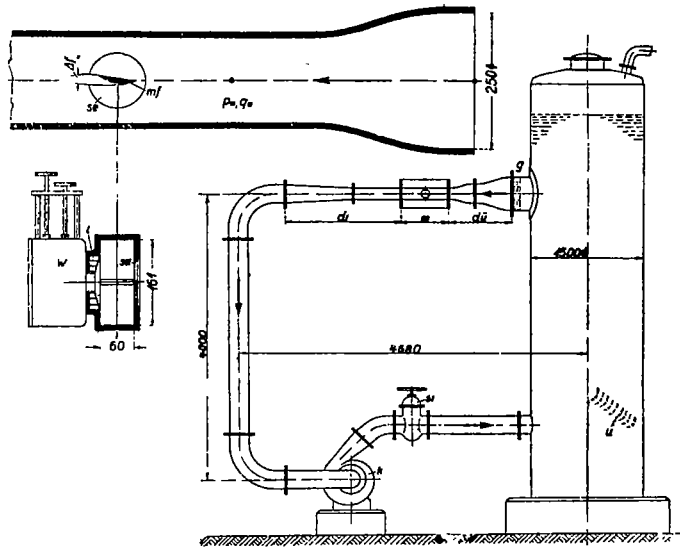


Fig. 1.



1. Suction-side cavitation starting at leading edge.



2. Suction-side cavitation starting at  $\approx 1/2t$ .



3. Pressure-side cavitation starting at leading edge.

Fig. 2.